JET–P(99)13

R D Gill et al

Direct Observations of Runaway Electrons during Disruptions in the JET Tokamak

JET–P(99)13

Direct Observations of Runaway Electrons during Disruptions in the JET Tokamak

R D Gill, B Alper, A W Edwards, L C Ingesson,
M F Johnson, D Ward.

JET Joint Undertaking, Abingdon, Oxfordshire, OX14 3EA,

Preprint of a Paper to be submitted for publication in Nuclear Fusion

August 1999

ABSTRACT

Runaways generated during disruptions in tokamaks may have damaging consequences in large machines because of the high power generated by their localized deposition on the vessel walls. In an investigation of the runaways generated in disruptions in JET, detailed time and space resolved X-ray images of the runaway beam in flight have been obtained for the first time and these allow a detailed diagnosis and analysis of the production and movement of the runaways. These measurements are now possible because of the development, for the JET D-T campaign, of radiation protected soft X-ray cameras. The measurements show that the runaways are generated at the vessel centre in a region with small minor radius and they then move to interact with a small area of the wall. The observed radiation power both in detectors installed in the torus and in the radiation protected cameras shows reasonable agreement with values calculated from the runaway current and energy. The current density profile and q-profile of the runaway beam are also determined. After the start of the disruption there is a delay before the onset of runaway generation and this may offer control possibilities.

1. INTRODUCTION

Tokamak discharges that disrupt often generate a runaway beam of electrons with a current which is a significant fraction of the total ohmic current[1]). This beam contains electrons with energies of many MeV and, because of its high total energy content, it can cause substantial damage when it hits the limiters or wall. There are serious concerns in the design of larger machines, such as ITER, of the possible consequences of this damage, and different schemes have been suggested to control or reduce these effects. The generation of runaways has received considerable theoretical attention and the general principles are well understood although there has been rather little detailed comparison with experimental measurements, especially for runaways generated in disruptions. Early theoretical work by Dreicer[2]) established the conditions for runaway production, while more recent work[3,4]) has emphasized the possibly important role of cascade processes. A model of the runaway production in disruptions has been development by Russo[5]) who found that the runaways should be preferentially generated at the plasma edge. In contrast the model of Jaspers[6,7]) predicts runaway generation in a small central region. However these models are critically dependent on the assumed plasma parameters during the disruption, and these are usually very poorly known.

The lack of confrontation between experiment and theory is due in considerable part to the absence of good diagnostic measurements of the properties of the runaway beams. In many tokamaks they only make themselves apparent when they hit the walls or limiters, producing copious gamma ray showers, and neutrons following γ-n nuclear reactions. However there are some measurements, of limited usefulness, of radiation from the runaways in flight. At JET the forward bremsstrahlung has been detected[8]) by indirect means and at Textor the synchrotron radiation emitted in the infrared has been used to determine the number, energy, pitch angle and

other features of the runaway beam[6,7]). The latter measurements have shown that the runaway beam is confined to a region of small minor radial extent. It has also been found that magnetic islands play a role in determining the structure and time development of the beam when runaway snakes have been observed[9]).

In this paper we wish to report new results which come from direct X-ray images of the runaway beam. These measurements provide detailed information on the time development of the runaways and the size, position and stability of the runaway beam. The current density and q-profile have also been determined. It has been found that there is a delay between the disruption and the start of the runaway generation. This delay offers a possibility of instigating runaway control methods.

In sect. 2 an overview of the runaway production process is given; the principal diagnostics are described in sect. 3; the experimental observations are presented in sect. 4; the electromagnetic radiation production mechanisms and the properties of runaway beam are discussed in sect. 5; conclusions follow in sect. 6.

2. OVERVIEW OF RUNAWAY PRODUCTION.

A variety of different limiter and wall materials have been used in JET: the machine was first operated without a divertor with plasmas formed in either a limiter, single or double null configuration. In the original configuration, with carbon wall tiles, disruptions were frequently followed by the generation of large runaway currents of more than 1MA which persisted sometimes up to several seconds. This was identified as corresponding to the plateau which developed on the current trace, and bursts of hard radiation, including neutrons, were observed when the current terminated as the runaways hit the torus wall. Around shot number 20000, the carbon tiles were changed for beryllium. This virtually eliminated disruptions with long runaway tails, reduced the total number of photo-neutrons produced, and decreased the rate of current decay in the post disruptive phase. These differences were attributed to different properties of the residual plasma following disruptions in the C and Be cases[10]). More recently, with the divertor configurations, very few disruptions with pronounced runaway tails have been found in surveys of the JET data covering more than 10000 shots. However, completely systematic surveys of this more recent data have not yet been carried out. The results in this paper were all taken with the Mark IIA divertor configuration.

The circumstances leading to plasma disruptions in JET have been discussed in detail in previous papers[1,11,12]) where it has been shown they are a consequence of operating the plasma too close to a boundary of density, inductance, pressure or safety factor. The details of the sequence of events before the current quench are well understood[1,11-13]) and an overview of the effect of the disruption on some of the main plasma parameters is shown in fig 1. Previous studies[1]) have shown that the plasma energy is lost in two stages; firstly at about two milliseconds before the negative loop voltage spike and again at the spike, itself a consequence of the changes in the

plasma current profile. Following this, the plasma current (I) decays quickly at a rate, $\tau^{-1} = R_p/L$, where R_p and L are the plasma resistance and inductance respectively. The loop voltage rises to a few hundred volts because of the substantial reduction in the plasma electron temperature, and possibly also because of an impurity influx which increases Z_{eff}. The high values of the loop voltage show that the plasma temperature must drop to between 5 and 20 eV. The control of the position of the current channel is almost always lost following a plasma disruption[11]). The loss of plasma pressure reduces the vertical field required for radial stability, but, as the vertical field cannot be changed on the required time-scale, the current column moves rapidly inwards. The stability in the vertical direction is also generally lost, particularly in very elongated plasmas. In fig 1, the position signals show that the current carrying column moves rapidly inwards and downwards and then hits the wall. In other shots the current channel sometimes moves inwards and upwards. The plateau which develops on the current decay trace about 10ms after the disruption is caused by the presence of runaways. The commencement time of the development of this current can be found from the departure of the current trace from a simple exponential decay. The runaways have a low electrical resistance and this makes the loop voltage start to fall about 6ms after the disruption. This delay, together with the delay seen on the current trace, confirms the suggestion made on other grounds by Ward[14]) that the runaways are generated only after a significant flux swing has taken place. It will be shown later in this paper that there is good further evidence for the delay from the soft and hard X-ray measurements. As noted by Ward, this will lead to a significant reduction in the maximum energy of the runaways that are generated. When the runaways hit the vessel walls, copious hard X-rays, gamma rays and neutrons are seen. The largest hard radiation spikes are found to be clearly correlated with large values of *dI/dt.*

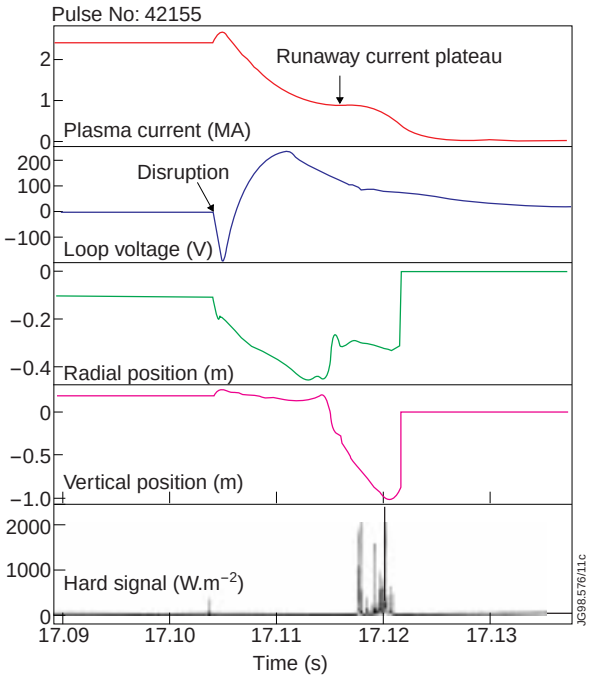

Fig.1: Overview of disruption showing the current and loop volts. The plasma radial and vertical positions are also shown and the bottom trace shows the burst of hard radiation produced when the runaways hit the vessel walls at about 17.12s.

The toroidal electric field, $\boldsymbol{E}_c$, applied at the plasma centre will be substantially higher than that observed at the plasma edge because of the poloidal flux between centre and edge. An estimate of $\boldsymbol{E}_c$ has been made with the simplifying assumption that the current has a uniform distribution after the negative voltage spike. It is found that $\boldsymbol{E}_c$ rises to more than 4 times the edge value to 45 V/m and then falls as dI/dt drops to zero.

The properties of the residual plasma following a disruption are not well determined. Interferometer measurements show that the electron density can rise substantially at a disruption to a maximum value of $5x10^{20}$ m^{-3}, but nothing is known about the composition of this plasma, although the pre-disruption values are a possible guide. Typical pre-disruption values for the discharges considered in this paper are ™n_e = $5x10^{19}$ m^{-3}, Z_{eff} = 2.2 mainly due to low Z impurities, and n(Ni)/n_e = $2x10^{-5}$. In addition the torus gas pressure 200ms after the disruption is measured to be 0.0026mBar, corresponding to a uniform density of $1.4x10^{19}$ m^{-3}.

3. DIAGNOSTICS

3.1 Radiation protected cameras

Most of the measurements reported in this paper were made with the JET radiation protected soft X-ray cameras[15]). These consist of a pair (to be called R4 and R8) of radiation protected cameras mounted at toroidally opposite positions in the median plane in octants 4 and 8 respectively. These cameras were built to detect X-rays during the D-T campaign of JET and each consists of 17 detector assemblies, shielded by about 0.8m of barytes concrete and steel. These view the plasma at an angle to the plasma current of 70^o through a common pinhole and a vacuum tight 250μm Be window. The lines of sight of the detectors are shown in fig 2. These are not quite straight lines as the cameras do not view the plasma in a radial direction and a projection is shown onto a radial cross-section at a common toroidal angle. Each assembly (see fig 3a) in R8 has a stack of detectors and absorbers facing the plasma as follows:

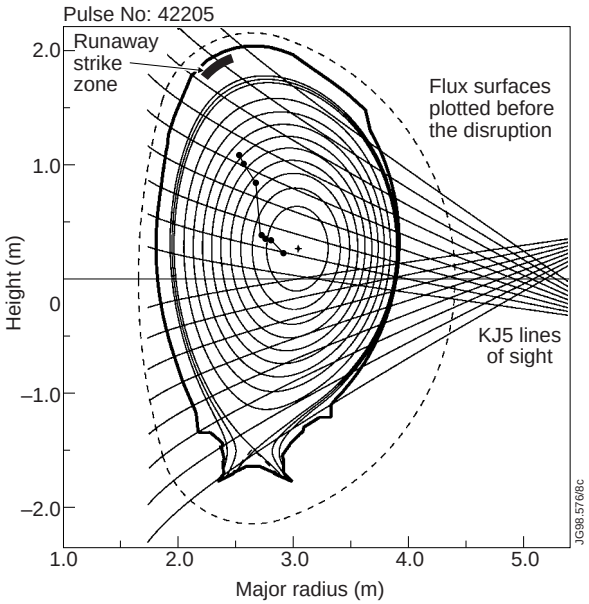

Fig.2: Cross-section of JET showing the lines of sight of the detectors of the radiation protected camera. The movement of the current channel following a disruption is shown by the dots, timed from the negative voltage spike at 2ms intervals. The strike zone on the upper inner wall is marked.

- a 14x14mm Si diode detector (called S1) to measure X-rays in the region 2 to 14keV;
- a stainless steel plate 2 mm thick to absorb all X-rays with an energy less than 50 keV;
- a second identical Si detector (S2) to measure the hard radiation component of the signal in the first detector produced by neutrons and gamma rays;
- a further stainless steel shield 19mm thick;
- a 20 cm long plastic scintillator - this plays no active role in the present experiments;
- a final identical Si detector (S3), which we shall refer to as the gamma ray detector, again detects hard radiation, but with reduced sensitivity compared with detector (S2).

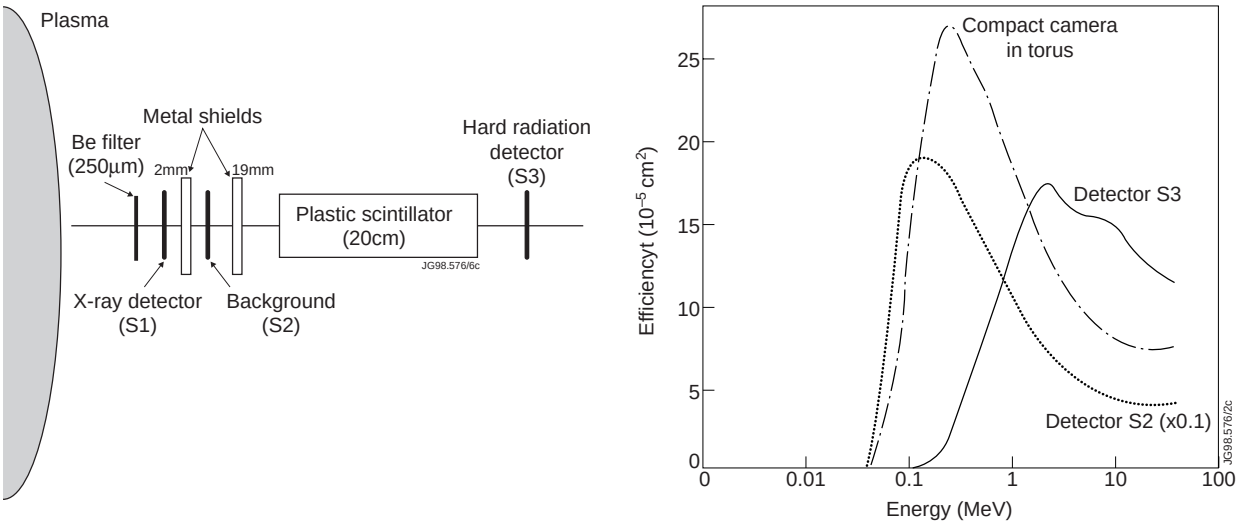

Fig.3:(a) The detector assemblies in the radiation protected camera are shown. Each assembly is shielded from hard radiation by at least 0.8m of barytes concrete and steel. (b) The efficiencies of the detectors are plotted as a function of gamma ray energy. The efficiency of detector S2 has been reduced by a factor of 10 before plotting.

The detector's relative efficiencies are shown in fig 3b. The latter have been calculated from the known photon cross-sections for the interaction of photons with Si and stainless steel as detailed in the appendix. The detector S2 has an energy threshold of about 50keV; S3 has a 140 keV threshold. Detector S2 is considerably more sensitive than S3. The detector assemblies in the R4 camera have only the first four items including detectors S1 and S2.

3.2 In torus detectors

In addition, measurements have been taken with a set of compact soft X-ray cameras[16]) (labeled A to J, and V) which are mounted in the torus in enclosed Inconel pipes (see fig 4). In normal discharges from D-D plasmas these detectors are used to measure the soft X-ray power per unit area from the plasma through a pinhole and thin Be window. This power is calculated from the measured detector current, the known Si power conversion factor of 3.6 W/A, and the detector etendue. However, if high energy gamma radiation is produced by runaway electrons, the detectors will also register a current generated by the gamma rays which penetrate the 5 mm thick Inconel pipes and camera cases. This current is processed by our software in the same way as for the soft X-ray signal to produce an apparent power. The

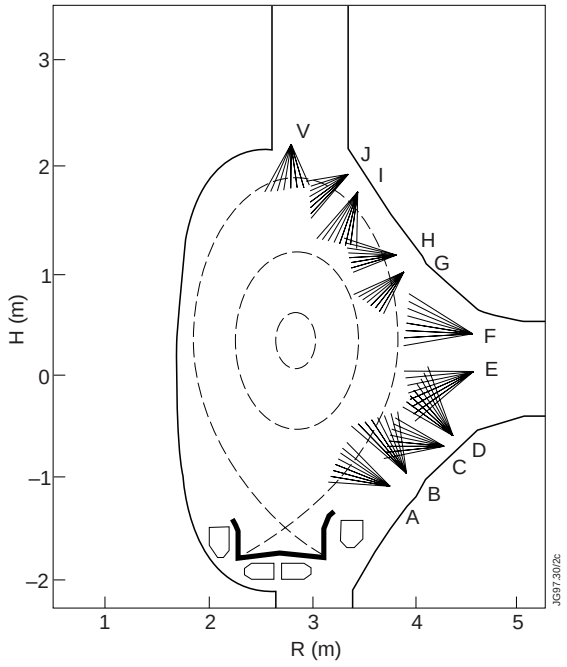

Fig.4: Fans of view and positions of the compact soft X-ray cameras V and A to J.

relative efficiency of these detectors is also shown in fig 3b. Data from all of these systems, and other diagnostics, has been taken with high time resolution (4μs) and good synchronization by the CATS[17]) data acquisition system.

4.0 OBSERVATIONS

A summary of the observations is first given for the runaways in flight from the time of the negative voltage spike to when they hit the wall. Two distinct effects have been seen: forward peaked bremsstrahlung gamma rays and line radiation produced by excitation of impurities. This is followed by details of some new features of the runaway-wall interaction.

4.1 Runaways in flight

The runaways in flight will produce bremmstrahlung with energy up to that of the runaways from interactions with the residual plasma. In earlier measurements this was observed by detectors outside the torus as a smooth background signal which was attributed to Compton scattering of the primary radiation[8]) from the port plates. The in-vessel detectors offer the opportunity of a much more direct observation of this bremsstrahlung. The signals from detector elements in cameras A to J typically show a very high intensity in one or sometimes two cameras with much smaller signals in all other cameras (fig 5). This is caused by the pronounced forward peaking of bremsstrahlung at relativistic energies which then illuminates only a restricted area of the wall. This immediately shows that the runaways must be confined into a region of restricted height. When the current channel moves up or down the signal of highest intensity moves from camera to camera allowing the approximate determination of the height of the illuminated area. If a more complete set of shielded detectors were to be installed around the outer side of the torus at intervals of a few cm, they could provide a detailed measurement of the size and movement of the runaway beam. Pairs of detectors, each with different radiation shields, could provide some information on the energy spectrum of the hard radiation.

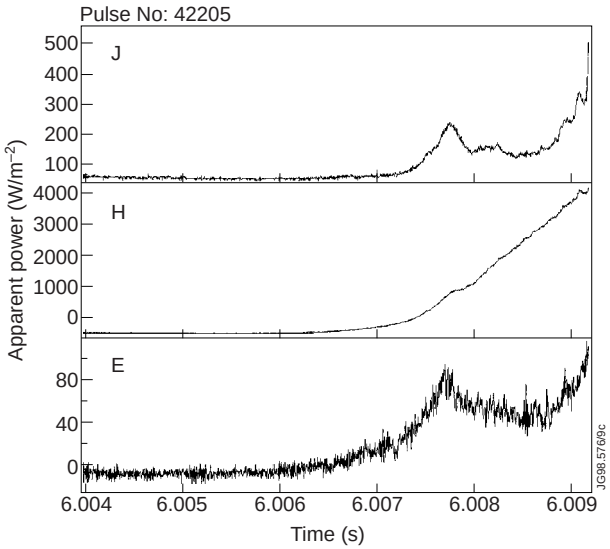

Fig.5: Apparent power observed in detectors of cameras E,H and J. The power in camera H is seen to be substantially larger than in its neighbours.

Before the runaways hit the wall, the intensity of hard radiation observed in the radiation protected cameras is very small, as to be expected. The bremsstrahlung produced by interaction of the runaways with the plasma or residual gas is concentrated into the forward direction and the intensity at the camera angle of 110^0 to the runaway electron direction is expected to be

extremely small, and orders of magnitude below our detectable limit. However, to our great surprise, there is a weak but clear image formed in the soft X-ray detectors S1(fig 6) and the movement of this image is always very clearly correlated with movement of the current channel determined from the position signals. Detailed examination of the data from many discharges has led to the inescapable conclusion that what is being seen, for the first time, is a direct image of the runaway beam. It is suggested that this image is formed by the runaways producing K-shell vacancies in metallic impurities in the residual plasma as will be discussed in sect. 5.2. This radiation would be emitted in all directions and not be confined to a narrow forward cone like the bremsstrahlung and would be detected with high efficiency. This image offers the possibility of determining several new properties of the runaway beam, and the vertical height can be immediately determined as a function of time. The measurements shows that the runaway beam starts in a small volume at the plasma centre and grows in diameter as it moves towards the wall but it never occupies more than a small fraction of the total volume. The vertical height of the beam is seen to increase from 30cm just after it first becomes visible to 80cm before it strikes the wall. The calculated height of the beam is rather insensitive to its major radius because of the rather large distance between the beam and the detector pinhole(3.2m). A delay between the negative voltage spike and the start of runaway generation is also seen. The smoothness of the emission suggests that the runaway beam is in a stable configuration until it hits the wall. Isolated toroidally symmetric hot spots (fig 6) are also sometimes seen. These have a harder component to their X-ray spectrum as they are also observed in detectors S2 which have an energy threshold of 50 keV. It is possible that they are caused by enhanced scattering of the runaways caused by small solid particles (UFO's) entering the runaway beam zone.

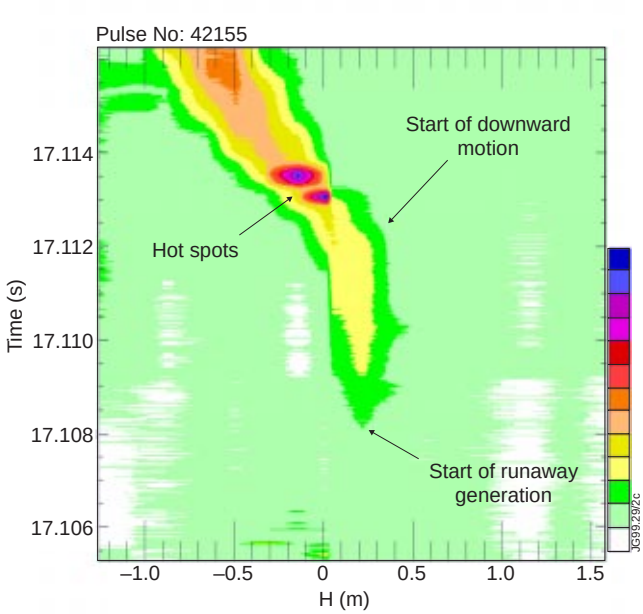

Fig.6: Soft X-ray image of runaways in flight. The pronounced downward motion is clearly seen. The runaways are first generated 4ms after the start of the disruption.

4.2 Runaway-wall interaction

The most pronounced effect of the runaway generation, seen on all tokamaks, is the generation of high power levels of hard radiation, gamma rays and some neutrons, when the runaways hit the vessel walls (see fig 1). Because detectors in cameras R4 and R8 are shielded from radiation not in their direct line of sight, it is possible to localize the interaction zone of the runaways as a small region with a poloidal width of less than 10cm of the upper or lower vessel depending on

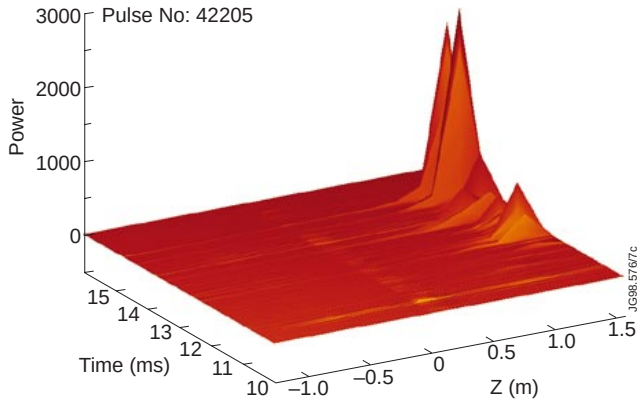

Fig.7: Runaway-wall interaction at the termination of the runaway beam. Large signals are generally observed in only one channel.

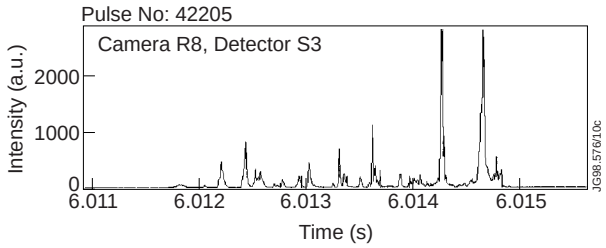

Fig.8: Time dependence of soft X-ray channel which directly views runaway strike zone. It is seen that there is a series of very fast spikes within an overall time window of 3ms.

the direction of the vertical movement of the beam. In fig 7 data from detectors S3 of camera R8 clearly show the extremely localized interaction zone, in this case in the upper inside of the vessel, in agreement with the position signals. The signals in the detectors S1 and S2 become overloaded by the high intensities at these times and do not therefore usually provide useful data. The runaway-wall interaction varies very rapidly with time (fig 8) and shows a series of very fast spikes, some less than 12μs half-width, within an overall time envelope of a few ms.

In a disruption examined in detail, the emission in flight measurements determine the diameter of the runaway beam at the moment of impact with the wall, as 0.8m. The centre of the beam has a minor radial velocity of 190 m/s and the runaways would therefore all hit the wall in 2.1ms, in good agreement with the value measured in this case of 2ms. It is therefore apparent that the runaway wall interaction is a simple consequence of the beam being driven into the wall at a uniform speed. The most probable explanation for the fast spikes is that the runaways have a very uneven spatial distribution on a series of concentric tori. This could be understood as a consequence of the extreme sensitivity of the production process to the ratio of the applied electric field to the Dreicer field. One could imagine that in the disruption, minor variations of E/E_D on different flux surfaces would lead to huge variations in the number of runaways produced. In addition if avalanche effects are important in the runaway generation process, it is possible that there are enhancements in the production rate on rational q-surfaces. In addition, the structure of the spikes is not toroidally symmetric, suggesting poloidal runaway current density variations on each flux surface. The runaway beam therefore appears to have a complex ribbon structure associated with the underlying poloidal field structure.

5. X-RAY AND GAMMA RAY PRODUCTION BY RUNAWAYS

Electromagnetic radiation is produced by runaway electrons when they are in flight, in collisions with the residual plasma, and also when they collide with the vessel walls. Very high power levels are produced in the wall interactions because of the high wall density compared

with the plasma. In both cases the predominant radiation production mechanism is bremsstrahlung and this will produce gamma radiation very strongly peaked in the forward direction of the runaways in a cone with half angle $1/\gamma$, where γ is the energy of the electron in units of its rest mass energy. Some of the radiation interacting with the wall will Compton scatter into other directions and will produce a weaker source of radiation which will be visible at angles outside the narrow cone.

Because the residual plasma contains many recombined impurity ions, there is also the possibility of K-shell vacancy production by the runaways. Metallic impurities such as nickel are known to be present in JET plasmas from spectroscopic measurements and their K-lines with energies in the soft X-ray range 5 to 8 keV will be detected with high efficiency.

5.1 forward Bremsstrahlung in flight

The bremsstrahlung is produced by runaway interaction with the residual plasma as has been discussed in ref[8]). In the absence of a poloidal field, runaway electrons moving in a circular orbit with major radius, R, would illuminate a restricted area of a wall at radius R_w (see fig 9) over a height $h = 2\, l/\gamma = (R_w^2 - R^2)^{1/2}/\gamma$ where l is the distance from the point of production to the wall. However, the effect of the poloidal field on the runaway orbit will be spread the radiation over a larger area. We consider a runaway beam on a toroidal surface with minor radius r where the poloidal field is B_θ . This beam will move around the toroidal surface in a direction tangential to that surface at a pitch angle $\phi_p = B_\theta/B_\phi = 2\text{x}10^{-7}\, I/\, r\, B_\phi$, with respect to the toroidal field. The bremsstrahlung from this beam of runaways will be within a cone with half angle $1/\gamma$, but the spot produced on the wall will move up and down both because of the position of the runaways on the toroidal surface and also because of the value of the pitch angle. These two effects will spread the radiation into a band on the vessel wall with a maximum height given by $H = 2\,(\, l\, B_\theta /B_\phi + l/\gamma + r)$. In subsequent calculations the total power emitted in bremsstrahlung will be assumed to be uniformly distributed over this band. This will allow for a good approximate calculation of the wall power without the need for a knowledge of the details of the distribution functions of the runaways apart from the average value of γ. Calculated values of H show that it is fairly independent of γ, strongly dependent on r at small values and strongly dependent on the total plasma current (figs 10a and 10b). Because there are several detectors mounted on the wall of the vessel it is possible, particularly in discharges where the runaway column moves smoothly up or down, to deduce an experimental value of H of 2m, in reasonable agreement with the calculation for values for r greater than 0.3m, $\gamma > 10$ and $I = 0.5$ MA.

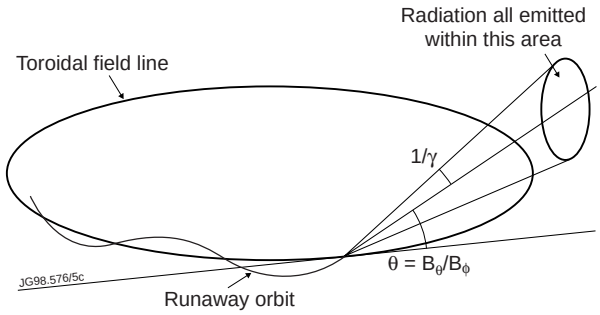

Fig.9: The forward cone of the bremsstrahlung and the runaway orbit are shown in schematic form.

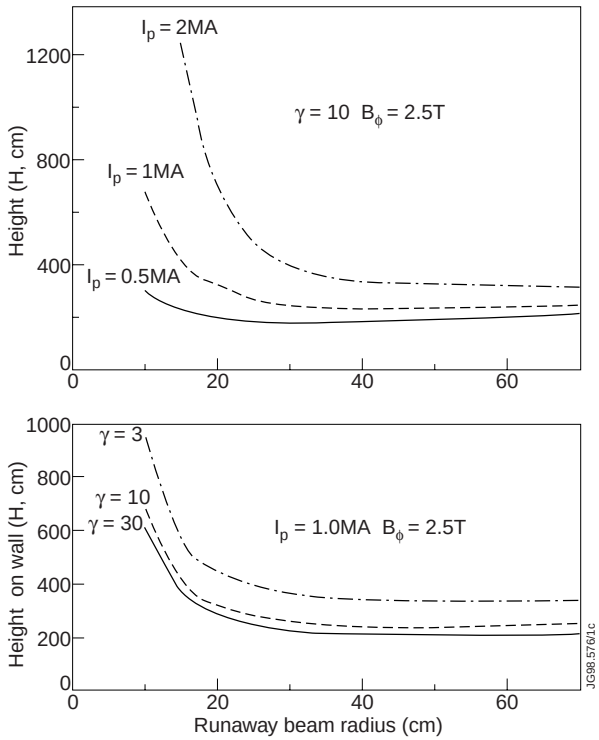

Fig.10: Values of the illuminated height on the outer vessel wall for different electron energies and currents.

The total bremsstrahlung power has been evaluated using the Heitler total cross-section[18]) for relativistic electrons, with screening by the plasma at distances greater than the Debye length, λ_D ;

$$\sigma(E_x) = 4\, Z^2 \alpha\, r_0^2\, h\, (1 + (p_f/p_i)^2 - 2\, p_f/3p_i)\, \ln(2\lambda_D/\alpha\, a_0)/\, E_x$$

where p_i is the initial and p_f the final momentum of the electron, a_0 is the Bohr radius, α the fine structure constant, r_0 the classical electron radius, E_x is the gamma ray energy, and h is Planck's constant. This equation is valid for $p_e, p_i > m_e c$. The total observed power in the detectors on the vessel walls may be found by integrating over the photon energy and summing over the ion species

$$P_D = \sum n_r\, n_z \int E\, \sigma(E)\, v_r\, \varepsilon(E)\, dE\, /2\pi\, R\, H$$

where v_r is the electron velocity, n_r and n_z are the runaway and ion particle densities, $\varepsilon(E)$ is the detector efficiency (fig 3b) given in the appendix. The calculated apparent detector power as a function of initial electron energy is shown (fig 11) for a set of sample parameters with a runaway current of 1 MA, a plasma density of 1×10^{20} m^{-3} and $Z_{eff} = 4.4$. These latter parameters are simply twice the pre-disruption values as there are no reliably measurements at these times. In the calculation the ion density is required and it is probable that some recombination may have taken place so that the experimentally determined n_e no longer reflects the density of the ions. The observed power is of the same order of magnitude as calculated for electron energies of 1 to 20 MeV. This essentially confirms the mechanisms proposed in this and the earlier paper[8]).

For non-relativistic energies a similar calculation has been carried out using the expressions given by Tucker[18]), except it has been assumed that the bremsstrahlung is isotropically distributed. It can be seen from fig 11 that there

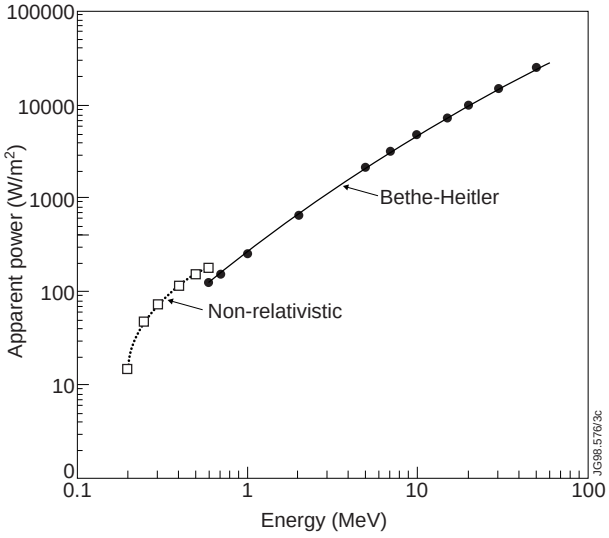

Fig.11: Calculated apparent detector power as a function of electron energy for selected plasma parameters.

is a reasonably smooth transition from the low energy to the high energy calculation. The figure also shows that the power is approximately linear with energy above about 1 MeV.

The observed radiated power can be calculated in more detail for detectors falling within the band of height *H* if the runaway current and energy are known as a function of time. The current may be taken from the departure of the current trace from a simple exponential decay. The runaway energy may be estimated from a free-fall calculation for an electron in the electric field $\boldsymbol{E}_c$ at the vessel centre assuming that the generation of runaways commences at the time when the runaways become visible on the current trace. By this time the electric field has already reached a large value for several ms and the maximum calculated runaway energy will be reduced because of this delay. Maximum energies of 35MeV are found. Without the delay this would be at least doubled. Using the linear curve of fig 11, the estimated values of the runaway current and electron energy, the time dependence of the signal in detector E has been derived. A comparison with the experimental values shown in fig 12 shows good agreement for a electron density of 2×10^{19}. It should be emphasized that there is an overall arbitrary factor in this calculation because of the uncertainty in the density and impurity content. However the low value of the density needed for agreement suggests that the runaway energy is overestimated. Detectors outside this band of height *H* would be expected to record a only small signal caused by Compton scattered radiation and the observed signals are typically smaller by a factor of 20.

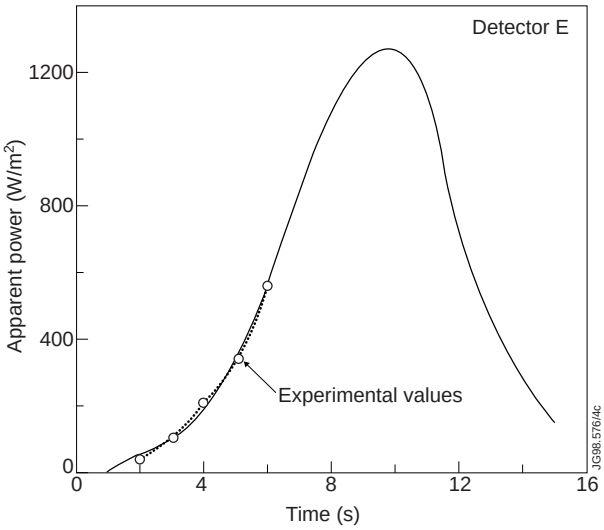

Fig.12: Comparison of experimental measurements with the calculated apparent power as a function of time using estimated values of the number of runaways and their energy.

The detectors of the R4 and R8 cameras are at angles of 110^{o} to the direction of the runaways and the bremsstrahlung will therefore have very low intensity. Because of the heavy radiation shield, the direct radiation component from the runaways only needs to be considered. This has been calculated to be only 1×10^{-4} W/m^2 , well below the detection threshold of 1W/m^2. It would therefore be concluded that no signal would be seen in these cameras from this source before the runaways hit the vessel walls.

The runaway energy spectrum may also be obtained from ref[4]) where an avalanche mechanism is proposed for the production of runaways in large tokamaks. The spectrum is quite different from that expected in free-fall calculations and has a exponential dependence on energy with an effective "temperature" of (17+3.4*Z*) MeV which is 25.5 MeV for Z=2.2. If the calculations shown on fig 12 were repeated with this value reasonable agreement would with

the measurements would be found for a slightly higher density of 2.8×10^{19}. Ref [4]) also gives an expression for the runaway growth time which is about 3ms for these particular JET discharges, and which compares reasonably with the experimental value of 2ms.

5.2 K - shell vacancy production

It is interesting and important to try to understand the other possible production processes leading to the emission of X-rays and in particular the processes leading to the formation of the image of the runaway beam seen in fig 6. The only plausible process is that of K-shell vacancy production by the runaways in the metallic impurity ions of the plasma remnants. The cross-sections (σ_z) for this process are large[20]), approximately $2\text{-}3 \times 10^{-26}$ m^{-2}, and rather independent of energy over a very wide range. In addition the X-rays produced by de-excitation into the K-shell have an energy, E_{Kz}, at which the camera detectors have almost 100% efficiency. We shall assume that σ_z can be treated as a constant and that n_z does not vary appreciably over the diameter of the runaway beam. If the runaway current density is j_r then the power produced by this process per unit volume is

$$P_K = \Sigma\, n_r\, n_z\, \eta_z\, \sigma_z\, v_e\, E_{Kz} = j_r \Sigma\, n_z\, \eta_z\, \sigma_z\, E_{Kz} / e$$

where η_z is the K-shell fluorescence yield (approximately 0.4 for nickel). The line integral signal observed by our detectors is

$$S_K = \int j_r\, dl\, \Sigma\, n_z\, \eta_z\, \sigma_z\, E_{Kz} / e$$

which shows that these are a direct determination of the line integrated runaway current density. In some cases the runaway beam moves very rapidly downwards, crossing an individual line of sight without substantial change and therefore allowing the determination of the emission profile. An example is shown in fig 13 where the profile is seen to be approximately gaussian. The abscissa has been changed from time to vertical distance using the measured vertical velocity of the runaway beam. It is seen that the beam has a full width at half maximum of 37cm, considerably larger than the instrumental resolution of 10cm. Inversion of this profile, assuming it to be circularly symmetric, determines the localized emission which is proportional to the current density profile. If the total runaway current is taken from the plateau value of the current trace, a q-profile can be calculated (fig 14) which shows that q rises from about 0.5 at the centre to 3 at the edge of the runaway beam. This distribution is similar to that found in a normal tokamak discharge and may account for the stability of the beam. An estimate may also be made of the edge q-value at the moment the runaways begin to hit the wall. The size of the beam can be estimated both from the soft X-ray image and the position signals. The total plasma current is assumed to flow within this region. This method gives reasonably consistent q-values of 3 at the edge of the runaway beam in several different discharges.

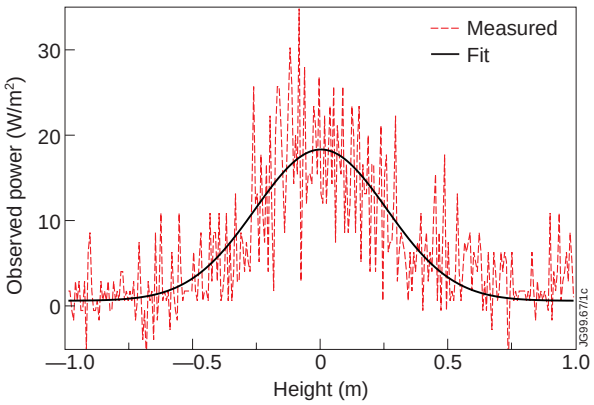

Fig.13: Emission profile determined from the signal from a single channel as the runaway beam passes rapidly across its line of sight. The fit to the data is also shown

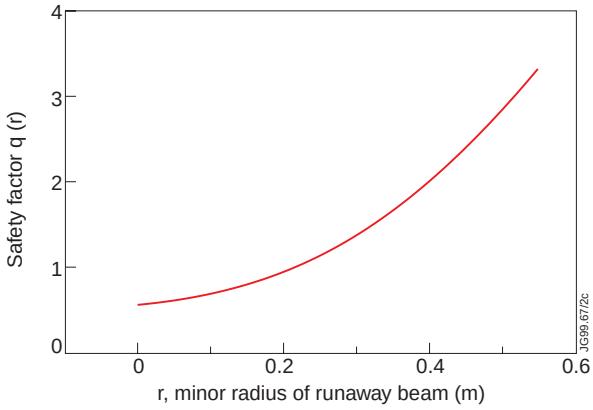

Fig.14: Safety factor profile of the runaway beam.

An approximate estimate of the observed line integrated X-ray power may be made assuming the runaway current density is uniform over a circular region of minor radius a_r . The signal intensity for a central view of the runaway beam is

$$S_c = 2\, I_r \Sigma\, n_z\, \eta_z\, \sigma_z\, E_{Kz} / \pi\, e\, a_r.$$

where I_r is the runaway current. As typical JET discharges contain almost equal concentrations of Ni, Fe and Cr this formula may be approximately evaluated just by considering the Ni component and setting η_z =1. A set of sample parameters I_r = 1 MA, $n_e = 10^{20}\ m^{-3}$, $n_z/n_e = 4\text{x}10^{-5}$ and a_r = 0.4m then gives S_c= 0.8 W/m^{-2}. Observed values are typically much larger at 30W/m^2 suggesting that the metallic concentrations in the post disruptive phase are considerably higher than our estimate from before the disruption. It is quite plausible that there is a large impurity influx in the early stages of the disruption.

6.CONCLUSIONS

The measurements reported in this paper give a detailed picture of the runaway beam generated in a disruption. The beam dimensions, its movement and stability have been determined and the localized nature of the interaction with the wall, in both time and position, is established. The measurements come mainly from the soft X-ray images which result from line radiation excited by the beam. The moment of onset of runaway generation, measured both from the plasma current and the X-ray image, is seen to be delayed after the negative voltage spike by about 5ms and this gives a possibility of preventing the generation of a large runaway current by acting during this time by the introduction of either killer pellets[21]) or liquid jets[22]) of H_2. The rapid fluctuations in the runaway-wall interaction has led to the conclusion that the beam is filamented. In addition, information has been obtained on the current profile of the runaway beam and its q-profile has been determined.

APPENDIX I

Calculation of the efficiency of the detectors for gamma rays.

Detectors installed in the cameras A to G and V in the torus detect gamma radiation after it has penetrated the Inconel, steel and copper detector housing. The penetration through this layer is estimated from the appropriate mass absorption coefficients (μ) and the known thickness of the housing. However only an average value of this quantity can be derived because of the different thickness of material traversed according to the route of penetration and the angle of incidence. This effect, investigated by repeating the calculation and allowing the material thickness to vary by 50%, makes only relatively minor changes to the threshold where the efficiency drops to zero. The energy absorbed in the detector is determined from μ and the detector mass. The results are plotted in fig 3b where a plot versus gamma ray energy of the ratio of power deposited in the detector to the incident power of the photons per unit area.

The efficiencies of the detectors in the detector assemblies of R4 and R8 have been calculated in the same way and are also shown in fig 3b.

REFERENCES

[1] Wesson, J. A., et al., Nuclear Fusion 29 (1989) 641

[2] Dreicer, H., Phys. Rev., 115 (1959) 238.

[3] Jayakumar, R., Fleichmann H. H. and Zweben S. J., Phys. Lett. A172 (1993) 447.

[4] Rosenbluth, M. N. and Putvinski, S.V., Nuclear Fusion 37(1997) 1355

[5] Russo, A. J., Nuclear Fusion 31 (1991) 117.

[6] Jaspers, R., Relativistic Runaway Electrons in Tokamak Plasmas, PhD thesis, Tech. Univ. Eindhoven, Netherlands (1995).

[7] Jaspers, R., Nuclear Fusion 36 (1996) 367.

[8] Gill, R.D., Nuclear Fusion 33 (1993) 1613.

[9] Entrop, I., Jaspers, R., Finken, K.H. and Lopes Cardozo, N. J., Runaway Snakes in Textor-94, Prague 1998; and plasma physics and controlled Fusion, to be published.

[10] Harris, G.R., Comparisons of the Current Decay during Carbon-bounded and Beryllium-bounded Disruptions in JET, JET-R(90)07, (1990).

[11] Tanga A. et al., Symposium on Plasma Engineering, San Diego (1991)69.

[12] Vanucci, A., and Gill, R. D., Nuclear Fusion 31(1991) 1127.

[13] Wesson, J.A., Ward, D. J. and Rosenbluth, M. N., Nuclear Fusion 30(1990)1011

[14] Ward, D. A., JET Joint Undertaking (1997), JET P(97)26

[15] Edwards, A. W., Alper, B. A., Blackler, K., Gill, R. D. and Lennholm, M., Diagnostics for Experimental Thermonuclear Fusion Reactors 2(1998)573 (Eds Stott, P. E. et al). Plenum Press, New York and London

[16] Alper B, et al, 21st EPS Conference on Controlled Fusion and Plasma Physics (montpellier) 3(1994)1304; and Rev. Sci. Instrum. 68(1997)778.

[17] Blackler, K. and Edwards, A. W., IEEE Transactions on Nuclear Science 41(1994)111
[18] Tucker, W.H., Radiation processes in Astrophysics, The MIT Press,(1975). Cambridge, USA.
[19] Taylor, P.A., Kellman, A.G., Rice, B.W. and Humphreys, D.A., Physical Review Letters, 76 (1996) 916
[20] Long, X., Liu, M., Ho, F. and Peng, X., Atomic data and Nuclear data Tables 45(1990)354
[21] Granetz, R.S., Fusion Energy (Proceedings of the 16th Conference on Fusion Energy, Montreal) 1(1996)757
[22] Rosenbluth, M.N., Putvinski, S.V. and Parks, P.B., Nuclear Fusion 37(1997).